Desalination 598 (2025) 118425

Contents lists available at ScienceDirect

Desalination

journal homepage: www.elsevier.com/locate/desal

Advanced desalination performance using PVDF electrospun nanofiber membranes across multiple membrane distillation configuration

Roberto Navarro-Tovar [a], Boya Qiu [a], Peter Martin [a], Patricia Gorgojo [b,c], Maria Perez-Page [a,*]

[a] Department of Chemical Engineering, The University of Manchester, Manchester M13 9PL, United Kingdom
[b] Instituto de Nanociencia y Materiales de Aragón (INMA), CSIC-Universidad de Zaragoza, Zaragoza 50018, Spain
[c] Departamento de Ingeniería Química y Tecnologías del Medio Ambiente, Universidad de Zaragoza, Zaragoza 50018, Spain

HIGHLIGHTS

- Electrospun nanofiber membranes exhibited high porosity (~93 %), high LEP (~3 bar), and superhydrophobicity (~150° contact angle).
- Electrospun nanofiber membranes displayed higher mechanical strength than commercial PVDF membranes.
- Electrospun nanofiber membranes were evaluated in three different Membrane Distillation configuration.
- Vacuum-assisted air gap membrane distillation outperformed other configurations, achieving 198 % higher flux and reduced energy consumption.

GRAPHICAL ABSTRACT

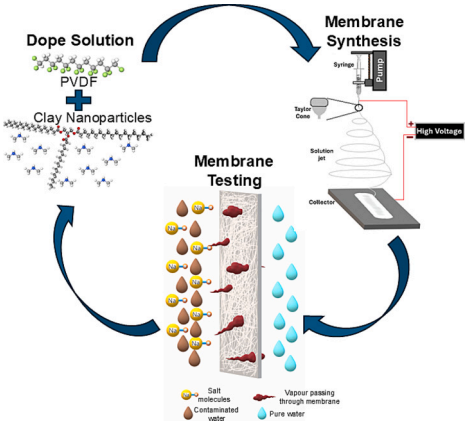

ARTICLE INFO

Keywords:
Membrane distillation
Desalination
Direct contact membrane distillation
Vacuum-assisted membrane distillation
Electrospun nanofiber membranes
Clay nanoparticle

ABSTRACT

This study reports the fabrication of polyvinylidene fluoride (PVDF) electrospun nanofiber membranes (ENMs) and their application across a range of membrane distillation (MD) configurations. Cloisite® 20 A (OMT) clay nanoparticles have also been successfully incorporated within the membrane nanofiber. The fabricated membranes exhibited notable MD performance enhancement, substantially increasing permeate flux rates compared with the membranes without nanoparticles, surpassing commercial PVDF membranes by 48 % and pristine ENMs PVDF membranes by 38 %. Additionally, the ENMs demonstrated significant improvements across all analysed parameters compared to pristine phase inversion PVDF membranes and with the PVDF mixed matrix membranes containing similar clay loading. Characterisations suggest that the superior performance is attributed to the formation of thinner fibers and the homogeneous dispersion of clay nanoparticles, obtaining high porosity (~93 %), high liquid entry pressure (~3 bar), good mechanical stability (~55 MPa of Young's Modulus) and surface superhydrophobicity (contact angle of ~150°). Stability tests over 5-day days confirmed these membranes' robustness, consistently maintaining rejection values above 99.9 %. In a comparative analysis of membrane configurations, vacuum-assisted air gap membrane distillation (VA-AGMD) emerges as the standout performer.

* Corresponding author.
E-mail address: maria.perez-page@manchester.ac.uk (M. Perez-Page).

https://doi.org/10.1016/j.desal.2024.118425
Received 20 October 2024; Received in revised form 2 December 2024; Accepted 6 December 2024
Available online 11 December 2024

The removal of air in VA-AGMD significantly improved process performance relative to direct contact membrane distillation (DCMD) and air gap membrane distillation (AGMD)—yielding a 55 % and 198 % increase in permeate flux and a 35 % and 58 % decrease in specific thermal energy consumption, respectively. A numerical model was successfully developed to predict the permeate flux observed experimentally from the ENMs, accurately determining the mass and heat transfer mechanisms in all MD processes. Comparison of permeate flux and thermal efficiency under identical conditions highlighted the model's reliability in capturing process performance. The use of the electrospinning technique has been found to be a promising approach to creating robust and high-performance MD membranes by taking advantage of the unique properties of nanofibers and clay nanoparticle fillers.

1. Introduction

Membrane distillation (MD) is an emerging separation process that, recently, has gained a lot of attention for applications such as water desalination. It operates based on liquid-vapour equilibrium, using vapour pressure difference, created by a temperature gradient, to induce the evaporation of volatile molecules, allowing them to pass through a hydrophobic porous membrane. As a means of desalination technology, MD has been extensively investigated in various applications, including the production of liquid food concentrates, the removal of dye from textile wastewater, the volume concentration of low-level radioactive wastewater, and the concentration of non-volatile acids [1–6]. The importance of MD lies in its ability to provide an environmentally sustainable solution to water scarcity when coupled with waste heat or renewable sources, especially in arid regions. However, membrane fouling, relatively low permeate flux, and the requirement to maintain a stable temperature difference across the membrane are ongoing limitations that researchers are actively working to overcome. Despite these challenges, MD is a promising technology with the potential to revolutionise water treatment processes and contribute significantly to global water sustainability efforts.

Membrane distillation has different configurations, each representing a distinct mode of operation to create the transmembrane vapour pressure difference. Direct contact membrane distillation (DCMD, Fig. S1b) involves direct interaction between a condensing fluid and the membrane on the permeate side, making it simple but prone to issues like wetting [7,8]. Air gap membrane distillation (AGMD, Fig. S1c) introduces an air gap between the membrane and a cooling surface, reducing heat losses [9]. Vacuum-assisted air gap membrane distillation (VA-AGMD, Fig. S1d) enhances AGMD by applying vacuum on the permeate side, significantly improving separation efficiency and permeate flux [10,11]. The configuration choice depends on the specific application, considering factors like flux, fouling resistance, and system simplicity, with each configuration presenting a trade-off between these considerations.

The membrane is critical in the MD process, working as a selective barrier that restricts the transport of undesired material from the feed, while facilitating the transport of vapour to the permeate side. The ideal MD membrane for water desalination must meet the following criteria: high hydrophobicity to repel liquid water, high porosity for efficient vapour transport, high liquid entry pressure to withstand wettability, and durability for prolonged operational use [1,2,12].

There are different membrane fabrication techniques for MD, such as stretching, phase inversion, and electrospinning, which will determine the membrane morphology and properties, which ultimately will have a direct effect in the MD performance [13,14]. The stretching process is suitable for semi-crystalline polymers like PTFE and PE, offering a solvent-free approach by heating the polymer above its melting point and extruding to the desired structure. Phase inversion relies on inducing a transition between two phases, driven by changes in polymer solubility. Electrospinning, considered highly effective for MD membranes, involves creating a randomly aligned polymer fibers network, delivering high porosity and interconnected pores. Each method brings unique features to the resulting membranes, influencing their applicability in different settings.

While different membrane fabrication techniques produce varying membrane structures, the challenges of wetting and fouling remain persistent in membrane distillation. Wetting occurs when liquid infiltrates the hydrophobic membrane pores, allowing contaminants from the feed side to permeate, compromising separation efficiency and reducing product quality [15]. This issue can become more pronounced in membranes with lower liquid entry pressure, regardless of their synthesis method. Conversely, fouling involves the accumulation of substances such as organic matter, salts, or microorganisms on the membrane surface or within its pores, leading to reduced permeability, lower permeate flux, and increased energy demands for the system [16].

Electrospinning techniques have emerged as a promising solution for addressing the limitations of traditional microporous MD membranes. Unlike conventional methods, electrospinning enables the fabrication of nanofibrous membranes with enhanced permeation flux, owing to their unique structure and high hydrophobicity [17]. This technology offers a scalable and cost-effective approach, leveraging the simplicity and versatility of the electrospinning process. Nowadays, continuous automated electrospinning equipment suppliers are available on both bench and industrial scales [18]. Despite their advantages, electrospun nanofiber membranes (ENMs) encounter several limitations that hinder their practical applications. One primary challenge is their lower mechanical properties, which make them susceptible to deformation and damage under pressure [19]. Additionally, ENMs typically exhibit low liquid entry pressure, making them more vulnerable to wetting, particularly in harsh operating conditions [17].

To address these limitations, researchers are actively exploring new approaches in electrospinning to enhance membrane distillation performance and tackle critical challenges in water desalination. Zhao et al. [20] carried out the electrospinning technique to integrate three variants of metal-organic frameworks into MD membranes to eliminate ammonia-nitrogen from wastewater through DCMD configuration. They found that the membrane incorporating UiO-66-NH_2 exhibited the most superior performance. However, the formation of irregular fibers occurs due to the agglomeration of UiO-66-NH_2 particles, which results in a decline in membrane performance. Mutlu-Salmanli et al. [21] used electrospinning to integrate a PVDF nanofibrous membrane with polybenzoxazine (PBz) for use in a VA-AGMD process. After curing, the water contact angle of the PBz-blended PVDF membrane increased by 30° compared to the pristine PVDF membrane, indicating enhanced hydrophobicity. However, the liquid entry pressure (LEP) values of the PBz-blended membrane remained similar to those of the pristine PVDF samples, staying below 1 bar. Attia et al. [22] developed an electrospun membrane by combining electrospinning and electrospraying techniques. A beaded structure was created by spraying a mixture of non-fluorinated alumina (Al_2O_3) nanoparticles with a low concentration of PVDF polymer onto a base membrane made from PVDF. The modified membrane, with a beaded layer thickness of 7.8 μm and a total membrane thickness of 115 μm, demonstrated a 61 % increase in liquid entry pressure (from 1 bar) and a water contact angle of 154°. However, the main challenges in this process are ensuring the stability of the sprayed material on the membrane surface and maintaining membrane flux.

The addition of clay nanoparticles can enhance the mechanical

strength and increase the liquid entry pressure of the membranes while improving their overall performance in membrane distillation applications [22]. Clays have garnered significant attention to be used as fillers into mix matrix membranes (MMMs) for various membrane-based applications due to their high compatibility with polymers, abundance, tunable surface properties and ability to enhance mechanical strength for improved long-term stability [23]. Clay materials such as montmorillonite, kaolinite, halloysite, and zeolites are widely used in various chemical processes such as adsorption, membrane-bases process, for example gas separation, water treatment, and electrodyalisis [24–28]. These clays can change their properties when exposed to different chemicals. Leyva-Ramos et al. conducted a study modifying natural clay by adding surfactants to improve its ability to remove different contaminants from water. They discovered that the effectiveness of organoclays in adsorbing pollutants depends on the type, size, and amount of surfactant used, as well as how the surfactant molecules are arranged on the clay surface. However, one drawback is that environmental factors such as pH and temperature greatly influence their adsorption capabilities [29].

Our previous research [30] proved the enhancements in permeate flux for desalination using phase inversion PVDF membranes enhanced with clays, in particular with organomontmorillonite (OMT). The OMT membrane exhibited a 30 % improvement over pristine PVDF and a 12 % improvement over commercial PVDF membranes while maintaining stability and performance during five days against fouling conditions [30]. For instance, montmorillonite uses the organic surfactant dimethyl dehydrogenated tallow quaternary ammonium, making the nano clay structure more non-polar [31,32]. This property makes the material hydrophobic and enables significant interaction with polymers, thereby improving the nanocomposite properties. Building on these findings, we aim to explore the potential of electrospinning as an alternative synthesis technique to enhance membrane performance further. By incorporating OMT into the electrospun PVDF matrix, we anticipate further hydrophobicity and permeate flux enhancements, which are crucial for desalination applications.

This study highlights the exceptional performance of electrospun nanofiber membranes (ENMs) based on PVDF, demonstrating their potential for water desalination. The integration of Cloisite 20 A (organomontmorillonite, OMT) clay nanoparticles into the ENMs matrix has been also explored, revealing their significant impact across multiple membranes synthesis techniques, electrospinning and phase inversion [30]. To assess their performance, the membranes were evaluated across different membrane distillation configurations. High-angle annular dark-field scanning transmission electron microscopy and energy-dispersive X-ray spectroscopy were used to analyse the membranes' morphological structure. Other characterisation techniques, such as water contact angle, liquid entry pressure, porosity, pore size, and tensile testing analysis, were conducted to link MD membrane performance enhancement to their morphology and other structural properties. A numerical model was developed to predict the mass and heat transfer phenomena exhibited by electrospun nanofiber membranes in membrane distillation systems. This model was essential for quantifying the mass and heat transfer resistances, offering valuable insights into the underlying transport mechanisms. By identifying these resistances, the model improves our understanding of factors influencing MD performance, such as flux and thermal efficiency, while guiding the optimisation of membrane materials and process configurations for future advancements. This innovative approach offers promising advancements in membrane technology to boost the water desalination.

2. Experimental section

2.1. Materials

All reagents and materials were used as received, and no modification has been done before the incorporation to the experiments. For the synthesis of the electrospun membranes the next chemicals were purchased: PVDF pellets with a molecular weight of ~534,000 g mol^{-1} were purchased from Sigma Aldrich, dimethyl sulfoxide (DMSO, ≥ 99.5 % pure) and acetone (≥ 99.8 % pure) were purchased from Fisher Scientific UK, and Cloisite20A® (Organomontmorillonte)(OMT) was obtained from Blagden UK. To prepare the artificial seawater solution, sodium chloride (NaCl, ≥99.0 %) was purchased from Merk. PVDF commercial membranes synthetised via phase inversion, with a nominal pore size of 0.22 μm and average thickness of 125 μm (GVHP09050) were purchased from Merck Life Science UK Limited.

2.2. Membrane preparation

The membranes were prepared by first dissolving the PVDF in a mixture of DMSO/Acetone with a ratio of 1:2 with OMT. PVDF with a concentration of 13 wt% of the total solution was used based on the maximum amount allowed in the electrospinning equipment to avoid precipitation/crystallisation or intermittent formation of the solution jet (Table S1 present the spinning outcomes involved with different polymer concentrations). As shown in Table S2, dope solutions with a total weight of 10 g were prepared by incorporating Solvent/OMT dispersions at 0.5, 2, and 4 wt% (based on the total weight of PVDF) into 1.3 g of PVDF pellets. These dope solutions underwent rigorous stirring for 12 h at 70 °C to ensure complete dissolution of the polymer. Subsequently, the solutions were left undisturbed for 2 h to facilitate the escape of trapped air bubbles, aiding in the degassing process.

The membranes were fabricated using the electrospinning technique through a LE500 Fluidnatek (Bionica, Spain), as shown in Fig. S1a. The prepared dope solution was transferred to a 10 mL syringe and placed in the syringe pump of the equipment. A constant flow rate of 3.5 mL h^{-1} was used. The distance between the nozzle and the plate was set at 10 cm, and an electric field of 15 kV was applied. The nozzle moved back and forth to obtain a membrane with a more even thickness and 13 × 30 cm membrane sheets were obtained. Once the dope solution was deposited, the membranes were allowed to dry overnight. A heat-press post-treatment was applied by placing the membrane between two tempered glasses (25 × 25 cm) weighing 784.1 g each, exerting a pressure of 10.66 N m^{-2}. The temperature used in the oven was 130 °C for 1 h to increase the fibers' mechanical strength, having a well-defined formation and cohesion of the interconnected pores. After post-treatment, the membranes were stored in plastic containers to prevent contamination and preserved until use.

To compare membrane synthesis techniques, mixed matrix membranes were prepared by dissolving PVDF in DMSO with addition of the OMT. The membranes were synthesised using the non-solvent-induced phase inversion (NIPS) technique, using the same procedure described by Navarro-Tovar et al. [30].

2.3. Characterisation of materials

High-resolution images of the membrane structure (Fig. 3) were captured using a FEI Talos F200A analytical electron microscope (AEM) high-angle annular dark-field scanning transmission electron microscopy (HAADF-STEM) operated at accelerating voltage of 200 kV. This setup was equipped with a Schottky field emission gun (X-FEG) operating at an extraction voltage of 4.5 kV, a monochromator (energy spread 0.25 eV) and an FEI Super-X 4-detector EDX system.

Surface functional groups were identified using Fourier-transform infrared spectroscopy (FTIR) with an attenuated total reflectance (ATR) accessory. The analysis was performed on a VERTEX 70v FT-IR spectrometer from Bruker. Spectra were gathered across the range of 400 to 4000 cm^{-1}.

The mechanical characteristics of the membranes were analysed through tensile strength and Young's modulus testing. Utilising an Instron 5542 tensiometer from Instron, equipped with a 100 N load cell, measurements were conducted under ambient conditions. For sample

preparation, rectangular strips of membranes (5 mm × 57 mm) were cut and positioned at each end between two paper window templates (25 × 57 mm) with exposed apertures of 15 × 25 mm in the middle of the paper template. The effective length of each sample was 25 mm. The elongation rate was set at 10 mm min^{-1}, and subsequent calculations yielded values for ultimate tensile strength and Young's modulus.

To assess dope solution viscosity, a rotational viscometer (Elcometer 2300, UK) was used. Three measurements were taken, and the average was reported.

Scanning electron microscopy with an energy-dispersive X-ray spectroscopy (SEM-EDX), liquid entry pressure (LEP), water contact angle (CA), thickness, porosity, and pore size distribution analysis were evaluated using the characterisation techniques described by Navarro-Tovar et al. [30] and briefly described in the supplementary information (Text S1).

2.4. Evaluation of the membrane within the MD set-up

Three different MD configurations were employed to assess the performance of the manufactured membranes, each having an effective area of 7.6 cm^2. In all instances, the hot feed solution (35 g L^{-1} of NaCl and 60 °C) underwent efficient circulation through the membrane module at a consistent flow rate of 1 L min^{-1}. To regulate the temperature of the cooling fluid at 20 °C, a Julabo F12-ED chiller circulated DI water through the module at a flow rate of 0.6 L min^{-1} and through a jacketed beaker in the case of DCMD.

In the AGMD setup, the membrane module, featuring a 3 mm air gap, where the permeate vapour transitioned into liquid form on the cooling plate. The resulting condensate exited the module by gravity and was collected in a measuring cylinder. For the VA-AGMD setup, the permeate module was connected to a vacuum pump, with a condensing trap positioned in the middle to collect the permeate. Each experiment involved filling the permeate container with 100 mL of DI water, and the conductivity was precisely measured using a digital conductivity meter (GO Direct Conductivity Probe). Additionally, a high precision scale (HCB 6001, Adam Equipment) was used to record the weight change measurement over time. Each MD configuration was analysed using a minimum of three membranes per material composition. The laboratory system diagrams for each MD are illustrated in Fig. S1.

Four parameters were evaluated to assess the performance for each MD configuration: permeate flux (J, kg m^{-2} h^{-1}), salt rejection (SR, %), specific thermal energy consumption (STEC, kWh m^{-3}), thermal efficiency (η, %), and gained output ratio (GOR). Table 1 shows the equations involved in analysing the MD performance. Thermometers were coupled at each exit of the MD module to measure the outlet temperatures.

2.5. Mathematical modelling of heat and mass transfer

To validate the experimental observations, mathematical modelling was employed to calculate heat and mass transfer for DCMD, AGMD, and VA-AGMD configurations. The model was developed using a numerical, iterative approach to solve a series of non-linear equations derived from the mass and heat balances governing the MD process.

Several studies have proposed models to predict the performance of MD systems, providing a valuable foundation for understanding heat and mass transfer mechanisms. A Matlab model was developed based on existing MD models from the literature, incorporating selected approaches from the literature [12,36–41]. The complete set of equations and detailed solution algorithms used for the numerical modelling are provided in the supplementary information (Text S2).

3. Results and discussion

3.1. Membrane characterisation

The morphology of the PVDF electrospun nanofiber membranes was evaluated by SEM. As shown in Fig. 1, it has been observed that all ENMs have a randomly oriented fibrous shape. The morphology of these nanofibers is directly affected by the concentration of the polymer, which impacts the solution viscosity (as shown in Table S2). At lower polymer concentrations, such as with PVDF 11 wt%, heterogeneous nanofiber networks are formed, as shown in Fig. S3. This is because the weak electrostatic forces struggle to overcome the surface tension, causing the polymer jet to break up into droplets and form beads. Additionally, the reduced viscosity of the dope solution at lower polymer concentrations leads to challenges in jet stretching and bending, resulting in irregular fibers [42,43].

On the other hand, a more uniform structure represented by adequate and straight nanofibers is observed at higher polymer concentrations (PVDF 13 wt%). The pristine PVDF exhibits an average diameter of approximately 0.49 μm. The incorporation of clay particles at concentrations ranging from 0.5 wt% to 4 wt% lead to a more irregular and thicker fibers, with diameters ranging from 0.56 to 0.74 μm (Fig. 2b, c, and d). Adding OMT to the electrospinning solution elevates viscosity (Table S1), impacting the flow behaviour and stretching of the polymer jet, ultimately contributing to the observed thickening of fibers.

EDX has been performed to estimate the presence of silicon (Si), magnesium (Mg) and aluminum (Al) on the membrane surface. Table 2 displays the content obtained, Si being the most predominant element. The concentration of these elements, especially Si, increases proportionately with increased clay loading in the membrane.

To confirm EDX results, FTIR was carried out to detect the presence

Table 1
MD performance parameters [10,12,33,34].

Parameter	Equation		Variables	Definition
Permeate flux (kg m^{-2} h^{-1})	$J_{exp} = \frac{\Delta m}{(\Delta t)A_m}$	(3)	Δm = change in the permeate mass (kg) Δt = sampling period (h) A_m = effective membrane area (m^2) C_P = permeate concentration (kg L^{-1})	Rate of permeate through the membrane per unit area.
Salt Rejection (%)	$SR = \left(1 - \frac{C_P}{C_F}\right) \times 100$	(4)	C_F = feed concentration (kg L^{-1}) m_F = feed mass flowrate (kg s^{-1}) C = feed specific heat capacity (kJ kg^{-1} K^{-1})	Membrane ability to prevent the passage of salts or solutes.
STEC (kWh m^{-3})	$STEC = \frac{m_F \times C \times (T_{F,in} - T_{F,out})}{F_D}$	(5)	$T_{F,in}$, $T_{F,out}$ = temperature of the hot feed stream at the inlet and outlet of the module (K)	Thermal energy required to produce certain amount of permeate.
η (%)	$\eta = 100 \times \left(\frac{J_{exp} \times A_m \times \Delta H_v}{m_F \times C \times (T_{C,out} - T_{C,in}) \times 3600}\right)$	(6)	F_D = distillate flowrate (m^3 h^{-1}) $T_{C,in}$, $T_{C,out}$ = temperature of the cold stream at the inlet and outlet of the module (K) ΔH_V = enthalpy of water vaporization (kJ kg^{-1})	Effectiveness of the thermal energy input that is converted into permeate.
GOR	$GOR = \frac{J_{exp} \times A_m \times \Delta H_v}{m_F \times C \times (T_{F,in} - T_{F,out}) \times 3600}$	(7)		Ratio of the energy content of the permeate to the energy input.

The physical properties (heat capacity, enthalpy of vaporization, and density) were estimated following the correlation in Sanmartino et al. [35], as shown in Table S3.

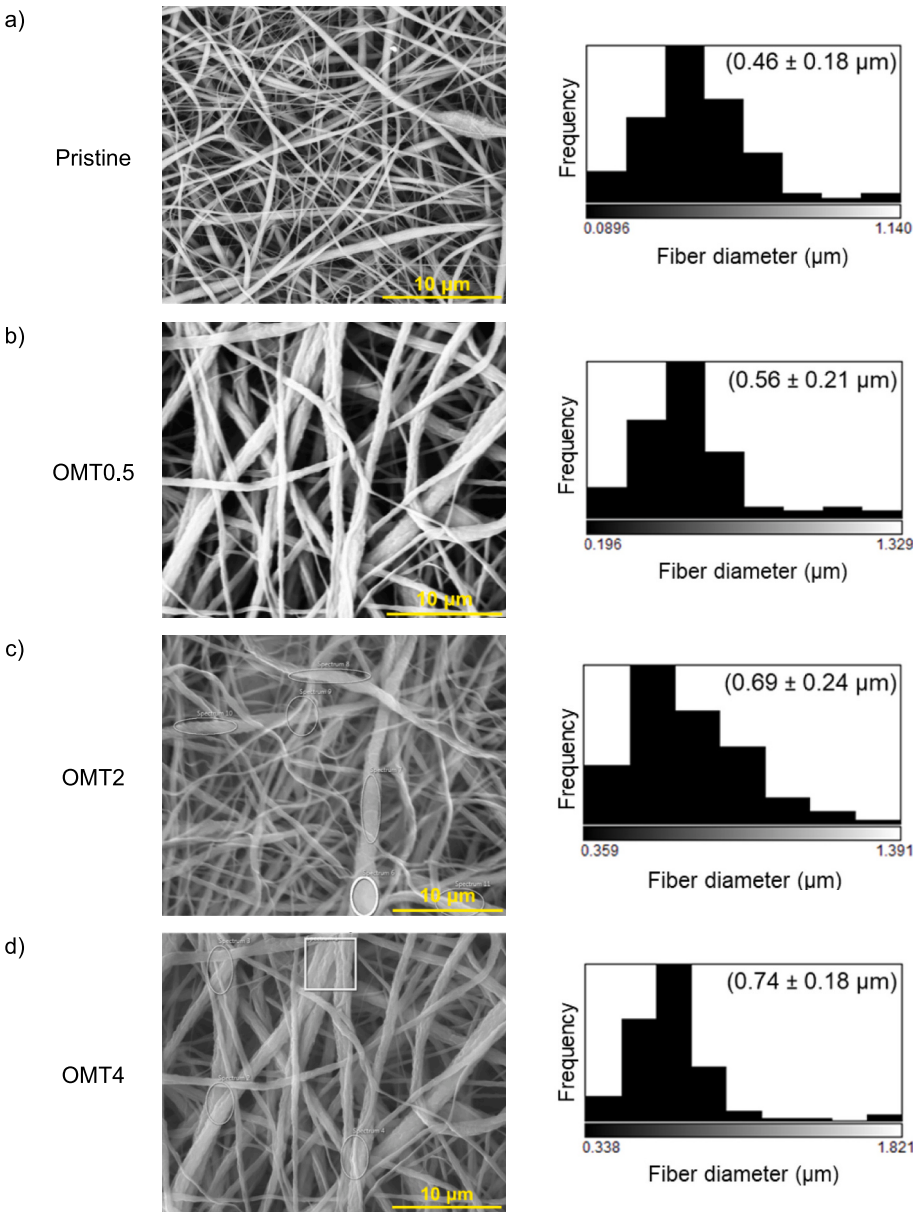

Fig. 1. SEM micrographs of the ENMs (PVDF 13 wt%) fabricated with their corresponding fiber diameter distribution and average fiber diameter.

of clay material within the membrane structure. Fig. 2 displays the FTIR spectra of PVDF-ENMs with control PVDF membrane and OMT loadings. The spectra show typical peaks at 750, 850, 1050, and 1150 cm^{-1}, which are present in all PVDF–OMT membranes, regardless of OMT loadings. These peaks indicate the presence of the α-phase characteristic peaks of PVDF. A representative intensity increase can be identified at 1000 cm^{-1} suggesting the presence of OMT Si—O stretching and bending groups. Additional peaks at 3600, 2900, and 2850 cm^{-1} were assigned to N—H stretching, C—H asymmetric stretching of methylene groups, and C—H symmetric stretching of methylene groups, respectively. The intensity of the N—H stretching peak increased proportionally with the content of clay particles, indicating the successful inclusion of clay particles into the nanofibrous membrane. A characteristic stretching vibration of the OMT carbonyl (C=O) group band was detected at ~1750 cm^{-1} suggesting the presence of the ester group in the dehydrogenated tallow. The FTIR analysis validates the successful integration of clay particles into the membrane, indicating a potential improvement in hydrophobicity.

A HAADF-STEM analysis was conducted to study the nanofiber structure and the dispersion of the OMT clay within the fiber. A fibrous structure was observed in the HAADF-STEM image (Fig. 3), indicating a well-formed nanofiber with a smooth and uniform appearance and free of significant defects. The brighter regions in the image, which correspond to higher atomic number elements, suggest that the OMT clay particles are well-dispersed within the nanofiber matrix. Without large clusters, the even distribution of these bright areas suggests a strong interfacial interaction between the clay and the nanofiber material. This effective dispersion is crucial for improving the composite's mechanical and thermal properties. The image has a sufficient resolution to observe nanoscale features, demonstrating that the introduction of OMT clay did not compromise the structural integrity of the nanofibers, thus preserving their mechanical strength and flexibility, as proved in the tensile strength measurements performed. Furthermore, according to STEM mapping, Si elements (main composition element in clay particles as shown in Fig. 3e and f) are evenly distributed in the nanofiber structure. This proves that Si can be uniformly dispersed in the PVDF-OMT ENMs with high dispersity.

One of the key limitations of ENMs is their reduced mechanical

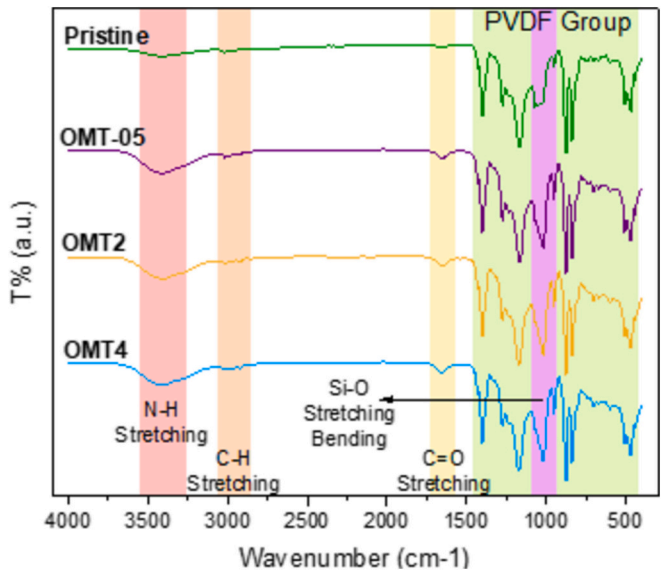

Fig. 2. FTIR-ATR spectra comparison of PVDF-ENMs for a) pristine and OMT at b) 0.5 wt%, c) 2 wt% and d) 4 wt%.

Table 2
EDX quantitative analysis of PVDF (13 wt%) and PVDF-OMT ENMs.

Surface elements (wt %)	Pristine PVDF (13 wt%)	PVDF-OMT (0.5 wt%)	PVDF-OMT (2 wt%)	PVDF-OMT (4 wt%)
C	51.0	53.0	50.5	46.3
F	47.7	44.0	42.2	39.9
O	1.3	1.0	0.8	0.7
Al		0.8	1.1	1.3
Si		1.1	5.3	11.7
Mg		0.1	0.1	0.1
Total elements	100	100	100	100

strength, which is attributed to their high porosity and the weak bonding between nanofibers [44]. This makes them more susceptible to mechanical deformation or damage under pressure compared to denser, less porous membranes. This is evident in Fig. 4, which illustrates the tensile strength (UTS) and Young's modulus (YM) of both commercial PVDF and pristine ENMs. The figure illustrates a notable decrease in both tensile strength (UTS) and Young's modulus (YM) for the ENMs compared to the commercial PVDF. However, incorporating OMT significantly enhances these properties, with the improvements becoming more evident as the clay loading increases (Fig. 4). This enhancement is attributed to the role of OMT as a nucleating agent, which increases the crystallinity of the PVDF matrix. The resulting higher crystallinity leads to improved mechanical properties, including increased tensile strength and Young's modulus [45]. The commercial PVDF membrane with a YM of 33 MPa and a UTS of 2.4 MPa demonstrates higher strength properties than the pristine ENM, which exhibits the lower mechanical properties of all membranes, with a YM of 12 MPa and a UTS of 0.9 MPa. Incorporating 4 wt% OMT into the ENM significantly enhances the mechanical properties compared to both the pristine ENM and the commercial PVDF membrane, achieving a YM of 55 MPa and an UTS of 4.3 MPa. Specifically, the membrane with 2 wt% OMT (OMT2) showed a 314 % increase in Young's modulus and a 303 % increase in ultimate tensile strength when compared to the pristine membrane. These improvements were even greater in the membrane with a 4 wt% OMT (OMT4), which exhibited a 453 % increase in YM and a 125 % increase in UTS, reaching a value of 4.3 ± 0.3 MPa. These enhancements are most likely due to the attractive interactions between the PVDF polymer chains and the layered structure with basal spacing of the OMT material. This interaction allows for the intercalation of various molecules or polymers between the layers, facilitating the inclusion of polymer chains that strengthen the bond between these materials. The observed mechanical improvements underscore the potential of OMT-loaded membranes for applications where superior mechanical strength is of utmost importance. Mechanical strength plays a crucial role in maintaining the structural integrity of a membrane during handling, installation, and operation. A robust membrane is less susceptible to damage from handling procedures, reducing the likelihood of defects that could degrade its performance. Good mechanical properties are essential to ensure that MD membranes are durable, reliable, and long-lasting, ultimately contributing to their overall performance and effectiveness in water purification applications.

High porosity values (typically exceeding 80 %) can benefit vapour transport in MD membranes [1,46]; however; factors such as membrane thickness (<60 μm) and low tortuosity (<1.2) [47] should also be considered to optimise overall performance. In this study (Fig. 5a), the porosity of all samples ranged between 85 % and 93 %, which is advantageous as high porosity provides a larger surface area for evaporation. A clear increase of the porosity can be observed comparing the commercial membrane with the pristine ENMs, however, the incorporation of OMT clay material leads to a porosity value exceeding 93 %, surpassing that of other electrospun fabricated membranes referenced in the literature ranging 81–92 % [48]. This increased porosity can be attributed to the influence of DMSO in the PVDF matrix. Compared with alternative solvents such as DMF or DMAC, DMSO exhibits higher Hansen solubility parameters and dielectric constant, enhancing electrospinnability, reducing bead formation, and producing thinner and more uniform fibers [43]. The modified clay material exhibits hydrophobic properties, leading to partial immiscibility (clay particles do not fully dissolve) within the hydrophilic DMSO-based dope solution. However, thorough mixing at high temperatures in DMSO facilitated adequate dispersion of the clay particles within the PVDF matrix. The interconnected nature of the nanofiber network further enhances porosity as adjacent fibers leave void spaces or pores. Electrospun fibers do not densely pack together, allowing gaps and voids between fibers to contribute to overall membrane porosity [49,50]. The ENMs exhibited an 8 % increase in porosity compared with those phase inversion membranes with the same OMT concentration prepared by Navarro-Tovar et al. [30]. This increase in porosity can be attributed to the electrospinning process, which produces a fibrous structure with interconnected pores, in contrast to the denser morphology formed through phase inversion. The random arrangement of nanofibers in ENMs creates more void spaces, leading to higher porosity and enhanced mass transfer potential in membrane distillation applications.

As depicted in Fig. 5b, the mean pore size of the membranes slightly reduced from 0.26 μm to 0.20 μm, along with a decrease in the maximum pore size from 0.43 μm to 0.39 μm, as the loading of OMT increased. This reduction in pore size is attributed to the coating of membrane fiber surfaces with OMT. Notably, the decrease in pore size was found to be proportional to the escalating loading of OMT. This trend holds significance for liquid entry pressure considerations, as a reduction in pore size can contribute to increase LEP. The densification of the membrane structure due to OMT loading can potentially enhance the resistance to liquid penetration, resulting in higher LEP. Therefore, the observed decrease in pore size, influenced by the progressive incorporation of OMT, may signify improved antiwetting properties of the electrospun nanofiber membranes. This connection between decreasing pore size and potential benefits for LEP underscores the intricate interplay between nanofiller loading, membrane morphology, and antiwetting characteristics.

ENMs exhibit liquid entry pressure (LEP) values in the range of 0.5 to 2 bar, a result of their open and interconnected fiber networks, which, while advantageous for high permeability and flux, offer less resistance to liquid entry [51]. As shown in Fig. 6a, the average LEP for all the prepared PVDF-OMT ENMs increases with the concentration of clay

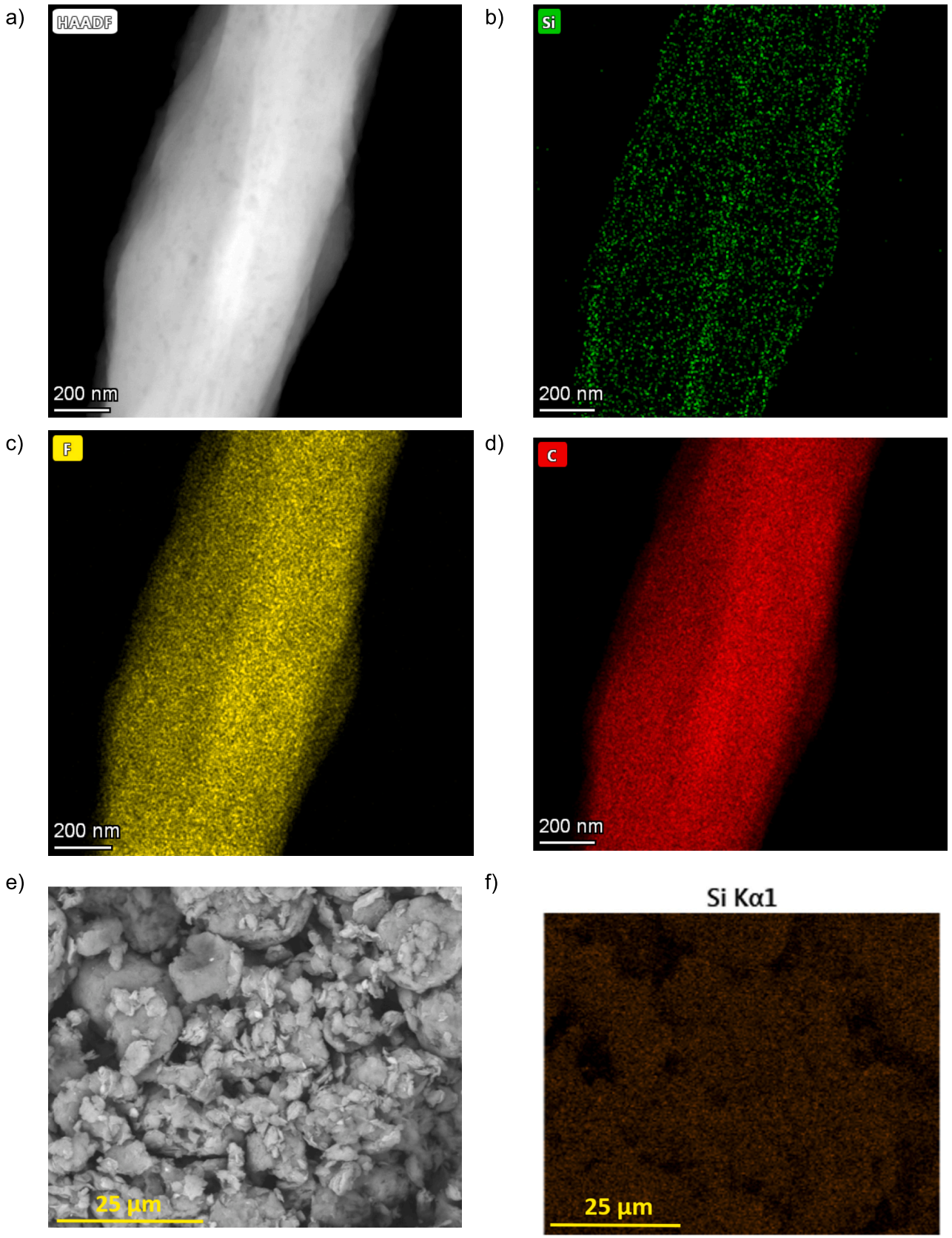

Fig. 3. HAADF-STEM image a) of electrospun PVDF-Clay composite nanofibers with 13 wt% of PVDF and 4 wt% OMT, and STEM mapping of Si, F, and C elements (b-d), and e) SEM micrograph and f) EDX analysis of OMT particles (x10000 magnification).

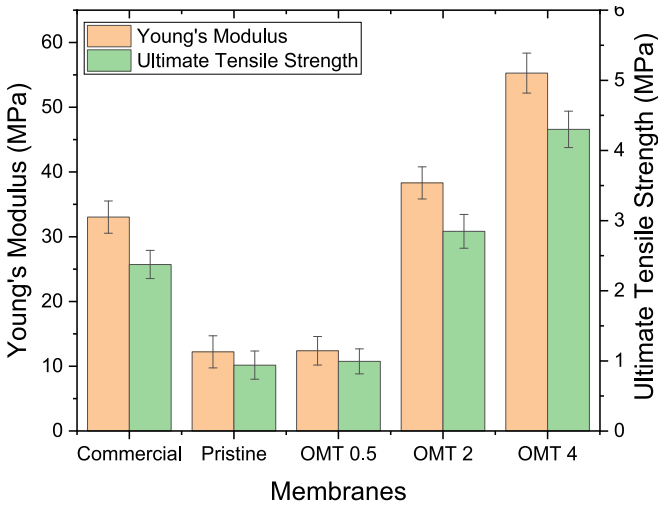

Fig. 4. Tensile strength measurements of all fabricated PVDF-OMT ENMs. Commercial PVDF has been made via phase inversion.

particles. Specifically, the membrane with the highest clay concentration (4 wt%) achieved a LEP of 3 bar. With an increase in the weight percentage of OMT, the membrane's porosity increases by 10 %, while the pore size decreases by 23 %. This relationship highlights the membrane's enhanced resistance to liquid penetration, resulting in a 50 % increase in LEP from 2 to 3 bar for OMT4. It is essential to compare this performance with a commercial PVDF membrane that exhibits a higher LEP of 3.5 bar. The superior LEP of the commercial membrane implies the higher values that phase inversion membranes can reach compared to ENMs. Phase inversion membranes typically exhibit LEP values ranging from 3 to 8 bar, reflecting their dense and uniform pore structure, which provides superior resistance to liquid penetration under higher pressures [19,30]. Understanding these differences is essential for selecting the appropriate membrane type based on the specific requirements of the MD process, such as operating pressure and desired separation performance. However, achieving an LEP of 3 bar for an electrospun membrane is noteworthy. Typically, electrospun membranes exhibit lower LEP values, making the obtained result a positive indicator of the membrane's liquid resistance capabilities. While the commercial PVDF membrane stands out in anti-wetting properties, the electrospun membrane's LEP of 3 bar highlights its competence, especially in contexts where electrospinning benefits such as high surface area and unique morphological features are crucial. The high LEP

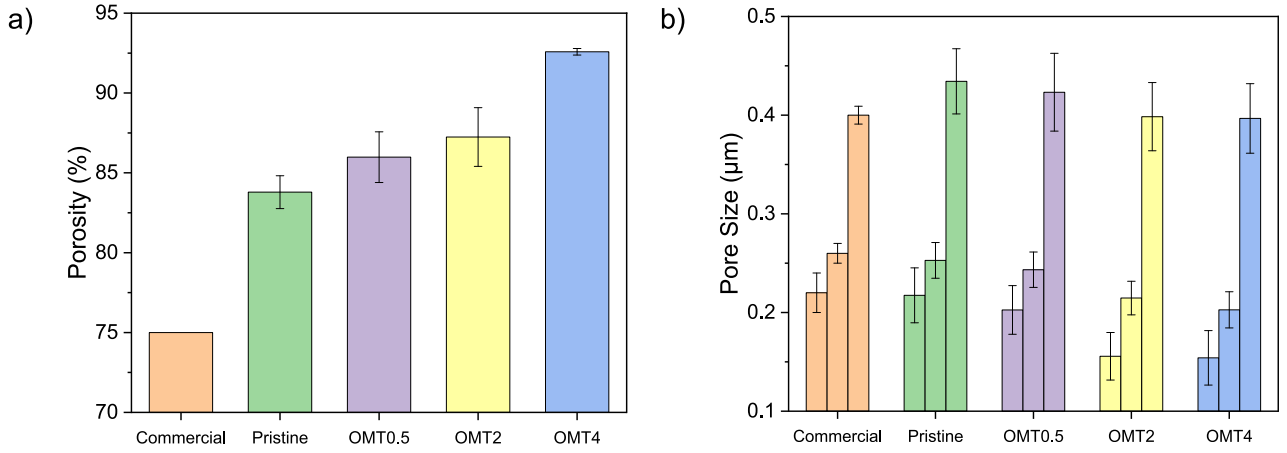

Fig. 5. Characterisation measurements of all fabricated PVDF-OMT ENMs, a) porosity, and b) pore size. From left to right, the bars indicated the smallest, mean and larger pore size obtained. Error bars represent standard deviations from three samples (or five in the case of the porosity). Right numbers of OMT stands for the concentration loadings.

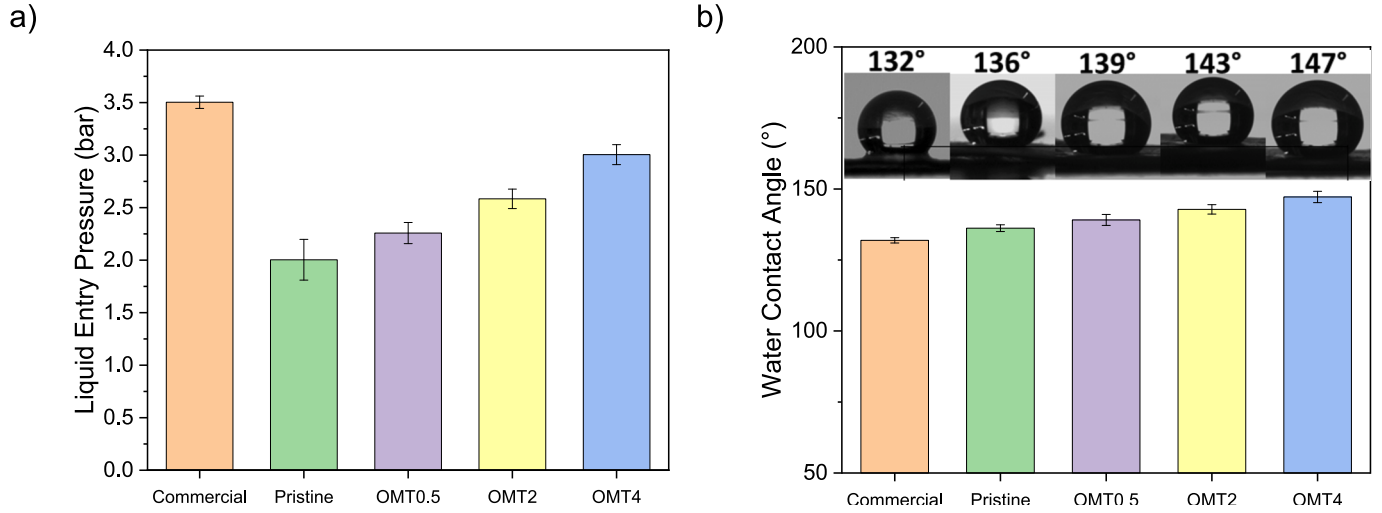

Fig. 6. a) LEP and b) water CA of fabricated PVDF-OMT ENMs. Error bars represent standard deviations from three samples.

observed in the OMT4 results from an effective balance between its small mean pore size, high porosity, and uniform pore distribution. The well-designed structure of the membrane allows for a high porosity level without compromising its ability to prevent liquid entry, which is crucial for sustaining the membrane's integrity and effectiveness during processes like membrane distillation, where both permeability and wetting resistance are essential.

The water contact angle (CA) of the prepared PVDF-OMT ENMs was measured and displayed in Fig. 6b. The results suggest that the hydrophobicity of the membranes increases with higher concentrations of clay. When the clay concentration reached 4 wt%, the membrane exhibited a contact angle of 147°, which is 11 % higher than the pristine PVDF membrane's contact angle of 132°. This indicates that including clay particles can significantly enhance the surface hydrophobicity of the membranes. Furthermore, the study demonstrates that a high concentration of 4 wt% of clay is optimal for producing membranes for membrane distillation. These findings provide valuable insights into the role of clay particles in improving the hydrophobicity of membranes and can inform the development of more efficient membrane distillation processes.

Table S4 summarizes the different properties evaluated for each membrane in comparison with the PVDF commercial membrane.

3.2. Membrane performance

In order to evaluate the potential of the membranes, they have been evaluated in different MD configurations, along with different operation parameters depending on the MD system. The membranes were first tested in VA-AGMD to identify the optimal OMT concentration. VA-AGMD was chosen to assess the mechanical strength of the membranes under vacuum conditions, which may potentially lead to a significant impact on their integrity. The electrospun nanofiber membranes, are susceptible to mechanical stress that may cause rupture or collapse structurally. This may lead to a decline in the efficiency and reliability of the MD process. However, OMT membranes are expected to perform better under these conditions than commercial PVDF membranes. As previously discussed, OMT membranes exhibit a remarkable 60 % increase in their mechanical properties, including Young's modulus and ultimate tensile strength, compared to commercial PVDF membranes.

Two different vacuum pressures, 50 mbar and 100 mbar, were used during testing, leading to different permeate flux performance for each membranes depending on the content of clay, as can be observed in Fig. 7. The choice of these vacuum pressures was deliberate, aiming to approximate conditions nearing total vacuum, allowing for an exploration of the membrane's performance under increasingly challenging conditions.

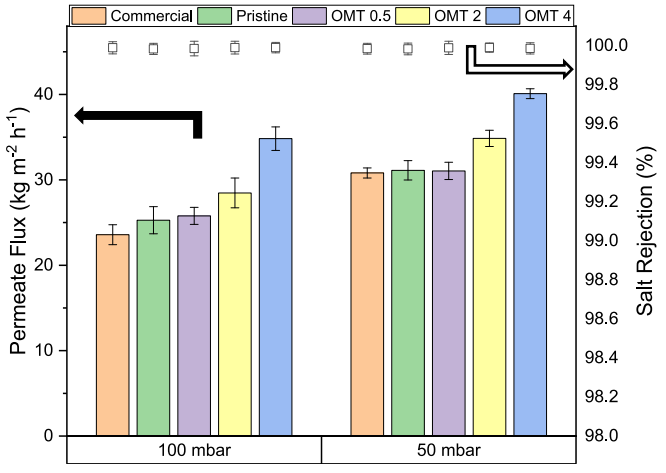

Fig. 7. Average total permeate flux of the prepared PVDF-OMT ENMs. Columns: permeate flux (kg m^{-2} h^{-1}), and square markers □: salt rejection (%). Error bars represent standard deviations from three samples.

Commercial PVDF membranes showed flux values of 30.8 (±0.59) kg m^{-2} h^{-1} at 50 mbar and 23.6 (±1.16) kg m^{-2} h^{-1} at 100 mbar. In comparison, pristine PVDF-ENMs outperformed their commercial counterparts, achieving flux values of 34.0 (±1.15) kg m^{-2} h^{-1} at 50 mbar and 27.7 (±1.38) kg m^{-2} h^{-1} at 100 mbar. This could be attributed to the creation of nanofibrous structures with higher and interconnected porosity, facilitating efficient vapour transport during distillation. Furthermore, electrospun membranes tend to exhibit higher hydrophobicity, a critical feature in MD to prevent liquid water ingress and enhance overall efficiency.

The clay-enhanced PVDF ENMs showed remarkable improvements in permeate flux. OMT4 was found to be the optimal concentration, exhibiting flux values of 40.1 (±0.58) kg m^{-2} h^{-1} at 50 mbar and 34.8 (±1.38) kg m^{-2} h^{-1} at 100 mbar, which is 30 and 38 % higher than the commercial PVDF membrane. This superior performance aligns with the hydrophobic nature of the OMT-enhanced membranes, indicating increased resistance to liquid penetration under vacuum conditions. Additionally, it is worth mentioning that all membranes consistently achieved salt rejections exceeding 99.9 %, affirming their efficacy in desalination applications.

A detailed comparison was conducted to evaluate the performance of membranes produced through different techniques, namely phase inversion (PI) and electrospinning (ENM), across three MD configurations: DCMD, AGMD, and VA-AGMD. The membranes tested include a commercial PVDF membrane, a phase inversion-synthesised OMT4 membrane (OMT4-PI), and an electrospun OMT4 membrane (OMT4-ENM). Table S5 summaries the results obtained for each membrane synthesis technique. This comprehensive analysis aims to clarify the unique performances of these configurations based on key parameters such as permeate flux, specific thermal energy consumption (STEC), thermal efficiency (η) and gained output ratio (GOR) (as shown in Fig. 8 and Table S6).

First, regarding DCMD, it was found that OMT4-ENMs had superior performance when compared to both Commercial PVDF and OMT4-PI. The OMT4-ENMs demonstrated a lower STEC of 3352 ± 418 kWh m^{-3}, combined with higher energy efficiency of 54.0 ± 2.46 % and a higher GOR of 0.22 ± 0.01, indicating enhanced energy efficiency and superior thermal performance. The higher performance of OMT4-ENMs can be attributed to the electrospinning process that creates a membrane structure with more interconnected pores and to their lower thermal conductivity, which is enhanced by incorporating clay nanoparticles like OMT [23,29,42,52–54]. This reduced thermal conductivity helps maintain a higher temperature gradient across the membrane, increasing the driving force for vapour transport and resulting in higher permeate flux [55]. Due to these characteristics, electrospun membranes outperform phase inversion membranes in MD applications.

In the AGMD process, OMT4-ENMs once again outperformed OMT4-PI and Commercial PVDF. The lower STEC (6465 ± 806 kWh m^{-3}), higher η (28.0 ± 2.73 %), and elevated GOR (0.11 ± 0.02) showed improved energy utilisation and superior efficiency in permeate production.

In VA-AGMD at 50 mbar, OMT4-ENMs performed exceptionally well, achieving higher permeate flux (40.1 ± 0.58 kg m^{-2} h^{-1}) with lower STEC (2169 ± 270 kWh m^{-3}), leading to superior η (83.4 ± 2.70 %) and GOR (0.26 ± 0.02). The vacuum assistance in VA-AGMD contributed to increased flux, while the reduced STEC showcased efficient energy consumption. This happens due to the withdrawal of non-condensable gases through vacuum assistance.

DCMD demonstrated an efficient desalination process, achieving a moderate STEC and respectable thermal efficiency. The gained output ratio was also noteworthy. The permeate flux was substantial, indicating effective vapour transport through the membrane in direct contact with hot and cold streams. On the other hand, AGMD results showed higher

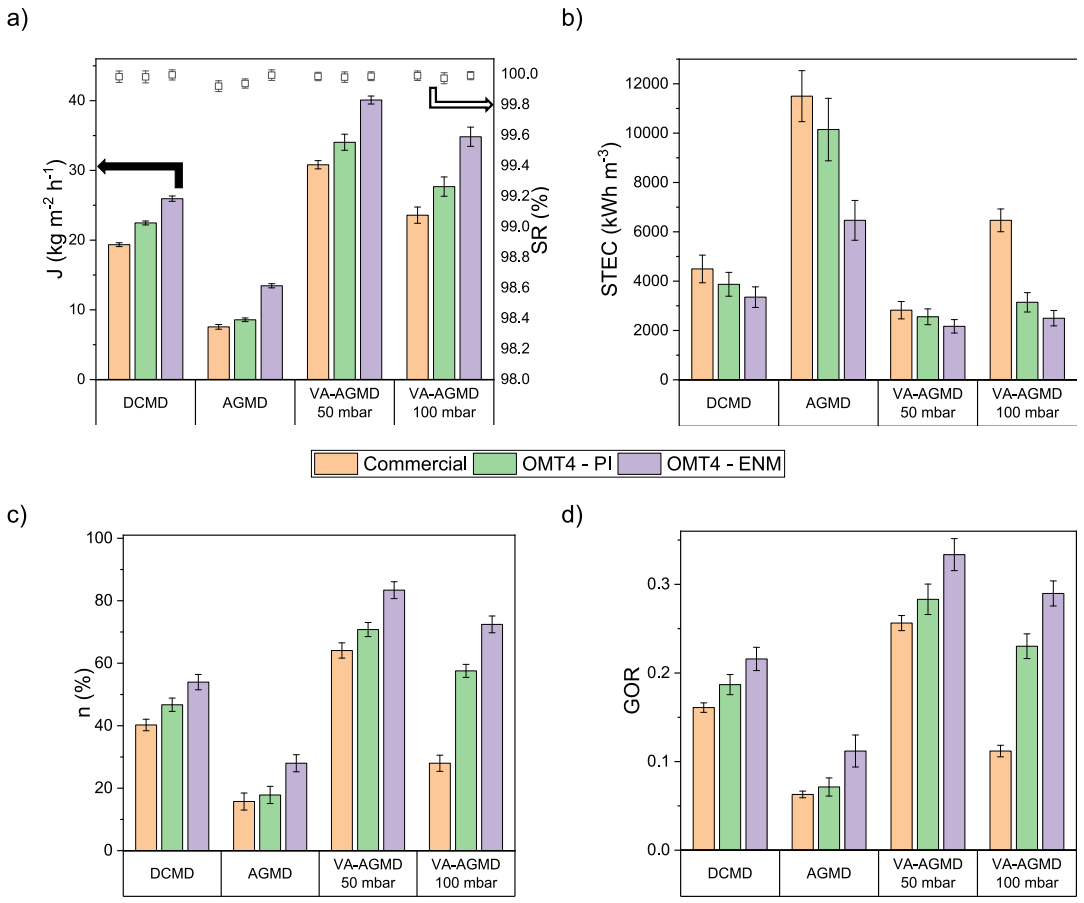

Fig. 8. MD configurations comparison, through a) permeate flux (kg m^{-2} h^{-1}), □: salt rejection (%), STEC (kWh m^{-3}), η (%) and GOR. Error bars represent standard deviations from three samples.

STEC values despite this configuration being associated with the MD configuration, which presents fewer heat losses. The lower permeate flux obtained in AGMD leads to higher STEC values than the other configurations due to the mass transfer resistance introduced by the air gap in the module, as permeate flux is inversely proportional to the STEC. However, VA-AGMD significantly improved desalination efficiency compared to AGMD, as it operated under a vacuum pressure of 50 mbar. The vacuum assistance facilitated the removal of non-condensable gases, enhanced thermal efficiency, and resulted in higher permeate flux and a higher output ratio.

The results show that the specific thermal energy consumption (STEC) for DCMD and VA-AGMD ranged from 2000 to 4000 kWh m^{-3}, while AGMD had a notably higher STEC of approximately 10,000 kWh m^{-3}. These findings indicate that our system's energy efficiency is lower when compared to the literature, which reports STEC values ranging from 400 to 2000 kWh m^{-3} [56]. The higher STEC values observed in our study are related to the elevated temperature gradient across the membrane, as shown in Fig. 8e. The temperature gradient, a critical factor influencing STEC, was higher in our experiments than those typically reported in the literature [10,34]. This more significant gradient leads to increased heat losses, which, in turn, elevate the overall thermal energy consumption. The heat losses in the system can be related to the material of the MD module. The module used in this study was constructed using Perspex material (Fig. S4), which may provide a different level of thermal insulation than materials used in other studies [57]. Poor insulation can lead to excessive heat dissipation, increasing the thermal energy required to sustain the MD process [58]. Modules constructed from materials with better insulating properties would likely reduce heat losses, contributing to a lower STEC. Hence, it underscores the critical importance of the MD system design.

DCMD is a process where the membrane is in direct contact with both hot and cold streams, allowing for a continuous flow of water vapour through the membrane. This configuration promotes efficient heat transfer, ensuring that the driving force for vapour transport is maintained. Nevertheless, it is essential to note that DCMD is comparatively less thermally efficient than other methods due to heat losses by conduction. On the other hand, AGMD introduces an air gap between the membrane and the cooling surface, minimising thermal losses and temperature polarisation. However, introducing this air gap adds another mass transfer resistance, hindering the permeate flux of the process. VA-AGMD outperforms DCMD and AGMD in terms of permeate flux, thermal efficiency, and gained output ratio. The introduction of a vacuum assists in removing non-condensable gases, such as air, from the membrane interface. This evacuation minimises the impact of temperature polarisation and enhances heat transfer efficiency, leading to higher permeate flux values. The vacuum pressure helps create a more favourable environment for vapour transport, overcoming potential limitations of the air gap in traditional AGMD; however, the energy costs of generating the vacuum should be weighed against the process efficiency gains, particularly when low-grade heat is available.

While DCMD can be advantageous due to its direct contact configuration, VA-AGMD, with the added benefit of vacuum assistance, addresses the limitations of both DCMD and AGMD, making it a superior choice for enhanced desalination performance. The vacuum helps mitigate the drawbacks associated with the air gap in AGMD, resulting in improved thermal efficiency and permeate flux. The optimal choice between DCMD and VA-AGMD depends on the specific requirements of the desalination process and the desired balance between simplicity and performance.

In summary, the comprehensive comparison of different MD

configurations has revealed the intricate interplay of parameters. OMT4-ENMs consistently outperformed their counterparts, underscoring the crucial role of fabrication methods in achieving superior MD outcomes. This analysis provides valuable insights for optimising MD configurations and highlights the importance of electrospinning in enhancing membrane performance for desalination applications, thereby contributing to the advancement of the field.

Table 3 shows a brief comparison between our study with previous results. The OMT4-ENMs membrane has a higher permeate flux than ZIF-71, which could be attributed to its higher porosity of 93 % compared to ZIF-71's 84 % [59]. The increased porosity of OMT4-ENMs suggests more void space available for fluid flow, facilitating higher flux. Additionally, the smaller pore size of OMT4-ENMs (0.2 μm) compared to ZIF-71 (1.05 μm) may contribute to enhanced selectivity and help prevent the intrusion of larger foulants, potentially reducing fouling. OMT4-ENMs outperform Al_2O_3 in terms of permeate flux as well [22]. This is because of OMT4-ENMs' higher porosity of 93 %, which provides more fluid flow pathways compared to Al_2O_3's porosity of 88 %. Moreover, the OMT4-ENMs membrane exhibits a higher water contact angle of 147°, which suggests better hydrophobicity and reduced fouling compared to Al_2O_3's angle of 154°. The same behaviour is observed for reduced GO [60]. This could be attributed to the significant LEP of 3 bar in OMT4-ENMs, which provides greater resistance to liquid penetration compared to rGO's LEP of 0.7 bar. Additionally, the higher water contact angle of OMT4-ENMs (147°) indicates improved hydrophobicity, which may reduce the adhesion of foulants and thereby help to minimise fouling compared to rGO's contact angle of 125°. All these factors collectively contribute to OMT4-ENMs' advantage in flux performance.

The OMT4-ENMs membrane demonstrates consistently superior performance in permeate flux compared to other membranes used in this comparison. This noteworthy achievement can be attributed to several key factors, namely higher porosity, smaller pore size, better hydrophobicity, and higher liquid entry pressure than most other membranes. These characteristics collectively contribute to enhanced fluid flow, reduced fouling, and improved selectivity, making the OMT4-ENMs membrane a promising candidate for various separation applications. Further research and development may uncover additional advantages and applications for the OMT4-ENMs membrane, consolidating its position as a competitive option in the field of membrane technology.

3.3. Model performance

The MD system model was first validated by comparing its predictions with other models reported in the literature [10,11,30,37–39,65–71]. As shown in Fig. 9, the developed heat and mass transfer model demonstrated good agreement, with deviations within ~10 %, across a range of system dimensions, flow rates, and operating temperatures. This validation highlights the model's reliability and robustness in accurately simulating MD performance under diverse conditions.

Furthermore, the developed model also matched well with experimental values. Minor differences observed can be attributed to experimental errors during the collection of distillate and inaccuracies in the measured temperatures used to calculate the theoretical mass flux. These factors are inherent challenges in experimental setups and were considered in the validation process.

Table 4 exhibits the calculated mass transfer coefficient (B_m) and total heat flux (Q_T) for various MD configurations and membrane types. The values of B_m represent the membrane's ability to transport vapour through its pores and are expressed in units of $kg\,m^{-2}\,h^{-1}\,Pa^{-1}$. The total heat flux ($Q_T$), expressed in $W\,m^{-2}$, reflects the energy required for vapour transport. These coefficients were derived based on the sum of the mass transfer resistances, which vary depending on the MD configuration, and were calculated following the algorithm outlined in the equations presented in Text S2.

The results demonstrate that the hybrid vacuum-assisted air gap MD configuration achieved higher B_m and Q_T values compared to DCMD and AGMD, particularly when using the OMT4-ENM membrane. This indicates the superior mass transfer and energy performance of the OMT4-ENM membrane in vacuum-assisted configurations, highlighting its potential for improved desalination efficiency. Additionally, the comparison between the experimental permeate flux (J) and the flux calculated using the mass transfer model showed strong agreement, with deviations consistently within an acceptable error margin. This further validates the robustness of the developed model and its applicability across different configurations.

4. Conclusions

The fabrication of PVDF-OMT membranes using electrospinning techniques has yielded significant insights into optimising membrane characteristics for enhanced performance. It was determined that a polymer concentration of 13 wt% PVDF in DMSO is optimal, leading to superior membrane properties and higher permeate flux than other concentrations tested. This finding underscores the critical importance of optimising polymer concentration to enhance membrane performance, providing a valuable reference for future research and practical applications in membrane technology.

Table 3
Comparison of the performance of the fabricated membrane with that of a previously reported electrospun nanofiber membranes in the literature.

Ref.	Main polymer	Additive	MD setup	Porosity (%)	Pore size (μm)	LEP (bar)	Contact angle (°)	ΔT (°C)	Flux ($kg\,m^{-2}\,h^{-1}$)
[59]	PVDFFcH	ZIF-71	DCMD	84	1.1	0.9	134	40	20.0
[42]	PVDF	SiO_2	DCMD	81	0.6	2.0	154	45	18.9
[61]	PS/PVDF	WO_3	DCMD	82	0.4	1.2	172	40	25.0
	PAN/PVDF-HFP-PS/PDMS	–	DCMD	78	0.4	0.4	149	40	27.7
[22]	PVDF	Al_2O_3	AGMD	88	0.4	1.7	154	40	18.6
[60]	PVDF	rGO	AGMD	–	–	0.7	125	45	30.0
[62]	PLA	–	AGMD	–	–	0.3	124	45	2.1
[63]	PVDF	Ho_2O_3	AGMD	91	–	–	132	40	12.2
[64]	PVDF	CB NPs	PVMD	–	–	2.2	151	40	2.5
[36]	PVDF	Fluorinated graphite	AGMD VA-AGMD (200 mbar)	76	0.3	3.3	157	30	3.2 15.9
[21]	PVDF	Mg/L benzoxazine	VA-AGMD (80 mbar)	71	0.4	0.9	133	45	19.3
This study	PVDF	OMT	DCMD AGMD VA-AGMD (50 mbar)	93 (±0.2)	0.2 (±0.1)	3.0 (±0.1)	147 (±2)	40	26.0 (±0.4) 13.5 (±0.3) 40.1 (±0.6)

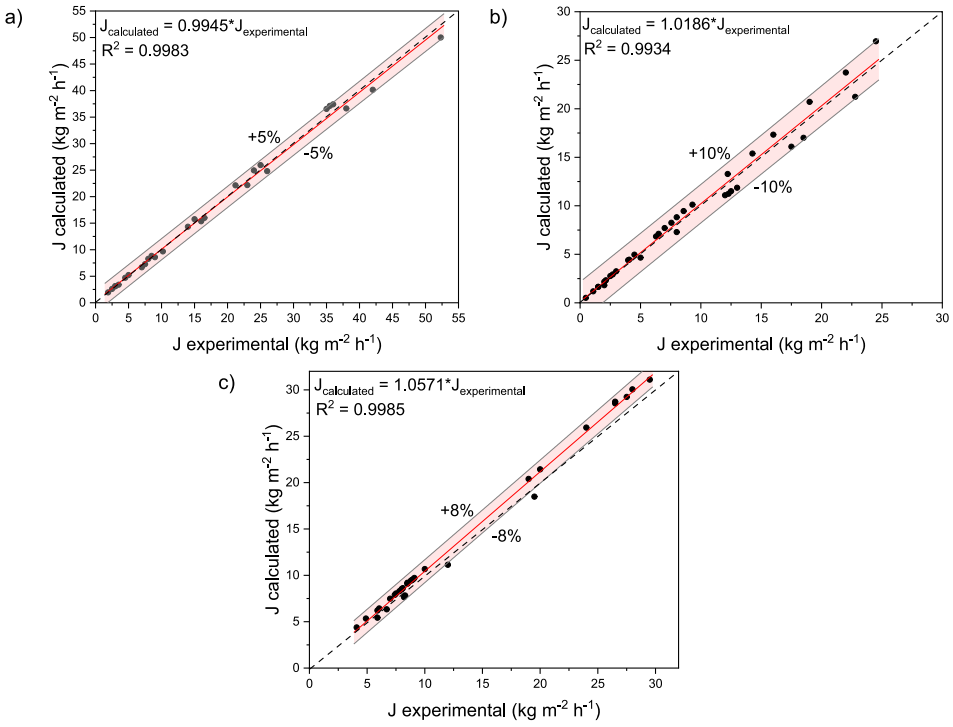

Fig. 9. Model prediction permeate flux results against experimental data in the literature for a) DCMD, b) AGMD, and c) VA-AGMD.

Table 4
Experimental permeate flux comparison against model and mass transfer coefficient and total heat flux calculations.

MD Configuration	Membrane	$J_{experimental}$ (kg m^{-2} h^{-1})	$J_{calculated}$ (kg m^{-2} h^{-1})	Error (%)	B_m x 10^{-7} (kg m^{-2} h^{-1} Pa^{-1})	Q_T (W m^{-2})
DCMD	Commercial	19.35	20.39	5.1	3.22	13,778
	OMT4 – PI	22.46	23.74	5.4	3.75	16,019
	OMT4 – ENM	25.95	27.35	5.1	4.32	18,462
AGMD	Commercial	7.56	8.44	10.3	1.33	5706
	OMT4 – PI	8.57	9.52	10.0	1.50	6433
	OMT4 – ENM	13.45	14.93	9.9	2.36	10,079
VA-AGMD (100 mbar)	Commercial	23.58	25.66	8.1	4.05	17,308
	OMT4 – PI	27.67	30.29	8.6	4.79	20,446
	OMT4 – ENM	34.83	37.91	8.1	6.00	25,678
VA-AGMD (50 mbar)	Commercial	30.81	33.57	8.2	5.31	22,699
	OMT4 – PI	34.03	36.91	7.8	5.84	24,914
	OMT4 – ENM	40.10	43.58	8.0	6.89	29,334

The integration of clay materials, particularly organo-montmorillonite, as has been anticipated by our previous work [30], has proven highly compatible (clay particles dispersed adequately) with PVDF polymers, making them effective for developing electrospun nanofiber membranes for membrane distillation. STEM and SEM-EDX analysis confirmed the uniform distribution of clay on the membrane structure. The incorporation of low concentrations of OMT significantly improved the porosity, mechanical properties, and liquid entry pressure (LEP), effectively addressing key limitations of ENMs-PVDF membranes. These improvements contribute to the overall stability and effectiveness of the membranes in filtration applications, highlighting the potential of clay-based additives to enhance polymer membrane performance.

Performance testing in membrane distillation experiments with saline feed solutions revealed that PVDF-OMT membranes with a 4 wt% clay loading achieved the highest permeate flux of 40.1 kg m^{-2} h^{-1} at a feed temperature of 60 °C. This was significantly higher than the fluxes achieved by commercial PVDF membranes and control samples, which recorded permeate fluxes of 30.8 and 31.1 kg m^{-2} h^{-1} under similar conditions (50 mbar in VA-AGMD). These results indicate that optimising membrane composition with clay additives can significantly enhance desalination efficiency, demonstrating the potential of this technology for industrial-scale applications.

DCMD is an effective and efficient desalination process that is suitable for situations where simplicity and effectiveness are essential. It has moderate STEC (~4000 kWh m^{-3}), commendable thermal efficiency (~50 %), and a gained output ratio (~0.2).

AGMD, has higher STEC values (~10,000 kWh m^{-3}) and is less energy-efficient than DCMD. It is also more challenging to use due to the air gap, but it may be useful in certain situations where its advantages (such as reduced fouling) outweigh its drawbacks.

The best performer in the analysis is VA-AGMD. The introduction of vacuum pressure is essential in overcoming the limitations of AGMD, resulting in higher thermal efficiency (~80 %), STEC (~2000 kWh m^{-3}), permeate flux (~40 kg m^{-2} h^{-1}), and GOR (~0.3).

However, the choice of a membrane distillation configuration ultimately depends on the desalination process's specific needs. Factors such as simplicity, efficiency, and the balance between thermal and operational parameters should be carefully considered. These findings provide valuable insights for optimising desalination processes based on configuration-specific advantages and trade-offs, taking into account the

importance of minimising STEC for improved energy efficiency.

The comparative analysis of PVDF-OMT membranes synthesised via phase inversion (OMT4-PI) and electrospinning (OMT4-ENMs) across three distinct MD configurations—DCMD, AGMD, and VA-AGMD—reveals a consistent trend of superior performance exhibited by the electrospun membranes. OMT4-ENMs consistently outperform OMT4-PI counterparts in all configurations regarding permeate flux, salt rejection, specific thermal energy consumption, thermal efficiency, and gained output ratio. This trend underscores the advantages of the electrospinning synthesis technique, highlighting its efficacy in enhancing membrane properties for membrane distillation applications.

The incorporation of OMT clay into PVDF membranes has led to marked improvements in structural integrity and water distillation efficiency across different MD configurations. Key enhancements, including increased liquid entry pressure (LEP), greater hydrophobicity (evidenced by higher contact angles), and optimized pore structure, have collectively elevated the membrane's performance under operational conditions. These advancements underscore the potential of clay-modified PVDF membranes for high-performance filtration and separation processes.

CRediT authorship contribution statement

Roberto Navarro-Tovar: Writing – review & editing, Writing – original draft, Visualization, Methodology, Investigation, Formal analysis, Conceptualization. **Boya Qiu:** Methodology, Visualization. **Peter Martin:** Writing – review & editing, Supervision. **Patricia Gorgojo:** Writing – review & editing, Supervision. **Maria Perez-Page:** Writing – review & editing, Validation, Supervision, Resources, Project administration, Methodology, Investigation, Funding acquisition, Formal analysis, Conceptualization.

Declaration of competing interest

The authors declare that they have no known competing financial interests or personal relationships that could have appeared to influence the work reported in this paper.

Acknowledgments

This work has been financially supported by the UK Research Council EPRSC with the Program Grant SynHiSel EP/V047078/1. Navarro-Tovar R thank the Mexican National Council of Humanities, Sciences and Technologies CONAHCyT for its financial support through project No. 773949.

Appendix A. Supplementary data

Supplementary data to this article can be found online at https://doi.org/10.1016/j.desal.2024.118425.

Data availability

Data will be made available on request.

References

[1] A. Alkhudhiri, N. Darwish, N. Hilal, Membrane distillation: A comprehensive review, Desalination 287 (2012) 2–18, https://doi.org/10.1016/j.desal.2011.08.027.
[2] F.A. Banat, J. Simandl, Desalination by membrane distillation: A parametric study, Sep. Sci. Technol. 33 (2) (1998) 201–226, https://doi.org/10.1080/01496399808544764.
[3] M.C. García-Payo, M.A. Izquierdo-Gil, C. Fernández-Pineda, Air gap membrane distillation of aqueous alcohol solutions, J. Membr. Sci. 169 (1) (2000) 61–80, https://doi.org/10.1016/S0376-7388(99)00326-9.
[4] M. Alberto, et al., Immobilized graphene oxide-based membranes for improved pore wetting resistance in membrane distillation, Desalination 537 (2022) 115898, https://doi.org/10.1016/j.desal.2022.115898.
[5] N.A.S. Muhamad, et al., A review of membrane distillation process: before, during and after testing, International Journal of Engineering Technology and Sciences 6 (2019) 62–81, https://doi.org/10.15282/ijets.v6i1.1549.
[6] X. Wen, F. Li, X. Zhao, Removal of nuclides and boron from highly saline radioactive wastewater by direct contact membrane distillation, Desalination 394 (2016) 101–107, https://doi.org/10.1016/j.desal.2016.05.001.
[7] S. Cerneaux, et al., Comparison of various membrane distillation methods for desalination using hydrophobic ceramic membranes, J. Membr. Sci. 337 (1) (2009) 55–60, https://doi.org/10.1016/j.memsci.2009.03.025.
[8] J. Phattaranawik, R. Jiraratananon, A.G. Fane, Heat transport and membrane distillation coefficients in direct contact membrane distillation, J. Membr. Sci. 212 (1) (2003) 177–193, https://doi.org/10.1016/S0376-7388(02)00498-2.
[9] S. Kalla, S. Upadhyaya, K. Singh, Principles and advancements of air gap membrane distillation, Rev. Chem. Eng. 35 (7) (2019) 817–859, https://doi.org/10.1515/revce-2017-0112.
[10] J.A. Andrés-Mañas, et al., Performance increase of membrane distillation pilot scale modules operating in vacuum-enhanced air-gap configuration, Desalination 475 (2020) 114202, https://doi.org/10.1016/j.desal.2019.114202.
[11] Z. Liu, et al., Experimental study of the optimal vacuum pressure in vacuum assisted air gap membrane distillation process, Desalination 414 (2017) 63–72, https://doi.org/10.1016/j.desal.2017.03.031.
[12] P. López-Porfiri, et al., *Towards the technological maturity of membrane distillation: the MD module performance curve.* Npj clean, Water 6 (1) (2023) 18, https://doi.org/10.1038/s41545-023-00234-0.
[13] L. Eykens, et al., Membrane synthesis for membrane distillation: A review, Sep. Purif. Technol. 182 (2017) 36–51, https://doi.org/10.1016/j.seppur.2017.03.035.
[14] M. Qasim, et al., Comprehensive review of membrane design and synthesis for membrane distillation, Desalination 518 (2021) 115168, https://doi.org/10.1016/j.desal.2021.115168.
[15] I. Tournis, et al., Superhydrophobic nanoparticle-coated PVDF–HFP membranes with enhanced flux, anti-fouling and anti-wetting performance for direct contact membrane distillation-based desalination, Environmental Science: Water Research & Technology 8 (10) (2022) 2373–2380, https://doi.org/10.1039/D2EW00407K.
[16] F. Ricceri, et al., Understanding the evolution of organic fouling in membrane distillation through driving force and resistance analysis, J. Membr. Sci. 686 (2023) 121993, https://doi.org/10.1016/j.memsci.2023.121993.
[17] R. Castro-Muñoz, A critical review on electrospun membranes containing 2D materials for seawater desalination, Desalination 555 (2023) 116528, https://doi.org/10.1016/j.desal.2023.116528.
[18] E. Aslan, et al., The electrospinning process, in: B. Bidanda, P.J. Bártolo (Eds.), Virtual Prototyping & bio Manufacturing in Medical Applications, Springer International Publishing, Cham, 2021, pp. 153–185, https://doi.org/10.1007/978-3-030-35880-8_7.
[19] M.O.S. Lobregas, et al., Advancing surface-enhanced electrospun nanofiber membranes: customizing properties for enhanced performance in membrane distillation, Macromol. Mater. Eng. 309 (7) (2024) 2300461, https://doi.org/10.1002/mame.202300461.
[20] L. Zhao, et al., MOF incorporated adsorptive nanofibrous membranes for enhanced ammonia removal by membrane distillation, Desalination 568 (2023) 117018, https://doi.org/10.1016/j.desal.2023.117018.
[21] O. Mutlu-Salmanli, et al., Fabrication of novel hydrophobic electrospun nanofiber membrane using polybenzoxazine for membrane distillation application, Desalination 546 (2023) 116203, https://doi.org/10.1016/j.desal.2022.116203.
[22] H. Attia, et al., Robust superhydrophobic electrospun membrane fabricated by combination of electrospinning and electrospraying techniques for air gap membrane distillation, Desalination 446 (2018) 70–82, https://doi.org/10.1016/j.desal.2018.09.001.
[23] R. Nisticò, A comprehensive study on the applications of clays into advanced technologies, with a particular attention on biomedicine and environmental remediation, Inorganics 10 (2022), https://doi.org/10.3390/inorganics10030040.
[24] Anadão, P., et al., Montmorillonite as a component of polysulfone nanocomposite membranes. Appl. Clay Sci., 2010. 48(1–2): p. 127–132, doi:https://doi.org/10.1016/J.CLAY.2009.12.011.
[25] G. Defontaine, et al., Nanoporous polymer – clay hybrid membranes for gas separation, J. Colloid Interface Sci. 343 (2) (2010) 622–627, https://doi.org/10.1016/J.JCIS.2009.11.048.
[26] N. Ghaemi, et al., Preparation, characterization and performance of polyethersulfone/organically modified montmorillonite nanocomposite membranes in removal of pesticides, J. Membr. Sci. 382 (1–2) (2011) 135–147, https://doi.org/10.1016/J.MEMSCI.2011.08.004.
[27] C.Y. Lai, et al., Preparation and characterization of poly(vinylidene fluoride)/nanoclay nanocomposite flat sheet membranes for abrasion resistance, Water Res. 57 (2014) 56–66, https://doi.org/10.1016/J.WATRES.2014.03.005.
[28] M. Rezaei, et al., Preparation and characterization of PVDF-montmorillonite mixed matrix hollow fiber membrane for gas–liquid contacting process, Chem. Eng. Res. Des. 92 (11) (2014) 2449–2460, https://doi.org/10.1016/j.cherd.2014.02.019.
[29] R. Leyva-Ramos, A. Jacobo-Azuara, J.I. Martínez-Costa, Organoclays., in: J. C. Moreno-Piraján, L. Giraldo-Gutierrez, F. Gómez-Granados (Eds.), *Fundamentals and Applications for Removing Toxic Pollutants from Water Solution*, in *Porous Materials: Theory and its Application for Environmental Remediation*, Springer International Publishing, Cham, 2021, pp. 341–363, https://doi.org/10.1007/978-3-030-65991-2_13.

[30] R. Navarro-Tovar, et al., Innovations in water desalination: enhancing air gap membrane distillation performance by the incorporation of clay nanoparticles into PVDF matrix membranes, Environ. Sci.: Water Res. Technol. (2024), https://doi.org/10.1039/D4EW00326H.
[31] P.H. Camani, et al., Impact of unmodified (PGV) and modified (Cloisite20A) nanoclays into biodegradability and other properties of (bio)nanocomposites, Appl. Clay Sci. 186 (2020) 105453, https://doi.org/10.1016/j.clay.2020.105453.
[32] P. Daraei, N. Ghaemi, Synergistic effect of Cloisite 15A and 30B nanofillers on the characteristics of nanocomposite polyethersulfone membrane, Appl. Clay Sci. 172 (2019) 96–105, https://doi.org/10.1016/j.clay.2019.03.002.
[33] H.C. Duong, et al., Evaluating energy consumption of air gap membrane distillation for seawater desalination at pilot scale level, Sep. Purif. Technol. 166 (2016) 55–62, https://doi.org/10.1016/j.seppur.2016.04.014.
[34] J.D. Gil, et al., Prediction models to analyse the performance of a commercial-scale membrane distillation unit for desalting brines from RO plants, Desalination 445 (2018) 15–28, https://doi.org/10.1016/j.desal.2018.07.022.
[35] Sanmartino, J.A., M. Khayet, and M.C. García-Payo, *Chapter 4 - Desalination by Membrane Distillation*, in *Emerging Membrane Technology for Sustainable Water Treatment*, N.P. Hankins and R. Singh, Editors. 2016, Elsevier: Boston. p. 77–109, doi:https://doi.org/10.1016/B978-0-444-63312-5.00004-8.
[36] H.F. Juybari, et al., Superhydrophobic composite asymmetric electrospun membrane for sustainable vacuum assisted air gap membrane distillation, Desalination 553 (2023) 116411, https://doi.org/10.1016/j.desal.2023.116411.
[37] O. Mutlu Salmanli, A. Yuksekdag, I. Koyuncu, Boron removal by using vacuum assisted air gap membrane distillation (VAGMD), Environ. Technol. Innov. 26 (2022) 102395, https://doi.org/10.1016/j.eti.2022.102395.
[38] O. Mutlu-Salmanli, et al., Boron removal and recovery via vacuum assisted air gap membrane distillation-crystallization (VAGMD-C): A pilot-scale study, Desalination 547 (2023) 116229, https://doi.org/10.1016/j.desal.2022.116229.
[39] S. Noamani, et al., Modeling of air-gap membrane distillation and comparative study with direct contact membrane distillation, Ind. Eng. Chem. Res. 59 (50) (2020) 21930–21947, https://doi.org/10.1021/acs.iecr.0c04464.
[40] S.O. Olatunji, L.M. Camacho, Heat and mass transport in modeling membrane distillation configurations: A review, Frontiers in Energy Research 6 (2018), https://doi.org/10.3389/fenrg.2018.00130.
[41] W.P. Parker, J.D. Kocher, A.K. Menon, Brine concentration using air gap diffusion distillation: A performance model and cost comparison with membrane distillation for high salinity desalination, Desalination 580 (2024) 117560, https://doi.org/10.1016/j.desal.2024.117560.
[42] J.A. Prince, et al., Preparation and characterization of highly hydrophobic poly (vinylidene fluoride) – clay nanocomposite nanofiber membranes (PVDF–clay NNMs) for desalination using direct contact membrane distillation, J. Membr. Sci. 397-398 (2012) 80–86, https://doi.org/10.1016/j.memsci.2012.01.012.
[43] F. Russo, et al., Innovative poly (Vinylidene fluoride) (PVDF) electrospun nanofiber membrane preparation using DMSO as a low toxicity solvent, Membranes 10 (2020), https://doi.org/10.3390/membranes10030036.
[44] L. Huang, et al., Improved mechanical properties and hydrophilicity of electrospun nanofiber membranes for filtration applications by dopamine modification, J. Membr. Sci. 460 (2014) 241–249, https://doi.org/10.1016/j.memsci.2014.01.045.
[45] D. Wei, et al., PVDF/palygorskite composite ultrafiltration membranes: effects of nano-clay particles on membrane structure and properties, Appl. Clay Sci. 181 (2019) 105171, https://doi.org/10.1016/j.clay.2019.105171.
[46] C. Skuse, et al., Can emerging membrane-based desalination technologies replace reverse osmosis? Desalination 500 (2021) 114844 https://doi.org/10.1016/j.desal.2020.114844.
[47] L. Eykens, et al., How to optimize the membrane properties for membrane distillation: A review, Ind. Eng. Chem. Res. 55 (35) (2016) 9333–9343, https://doi.org/10.1021/acs.iecr.6b02226.
[48] C.-Y. Pan, et al., Electrospun nanofibrous membranes in membrane distillation: recent developments and future perspectives, Sep. Purif. Technol. 221 (2019) 44–63, https://doi.org/10.1016/j.seppur.2019.03.080.
[49] L. Francis, F.E. Ahmed, N. Hilal, Electrospun membranes for membrane distillation: the state of play and recent advances, Desalination 526 (2022) 115511, https://doi.org/10.1016/j.desal.2021.115511.
[50] X. Gong, et al., Scalable fabrication of electrospun true-nanoscale Fiber membranes for effective selective separation, Nano Lett. 23 (3) (2023) 1044–1051, https://doi.org/10.1021/acs.nanolett.2c04667.
[51] M.O. Aijaz, et al., Anti-fouling/wetting electrospun nanofibrous membranes for membrane distillation desalination: A comprehensive review, Desalination 553 (2023) 116475, https://doi.org/10.1016/j.desal.2023.116475.
[52] S. Lakayan, et al., Electrospun polystyrene/Cloisite 20A fiber for selective separation of oil from water surface, J. Environ. Chem. Eng. 8 (4) (2020) 103775, https://doi.org/10.1016/j.jece.2020.103775.
[53] N. Awang, J. Jaafar, A.F., Ismail *thermal stability and water content study of void-free electrospun SPEEK/Cloisite membrane for direct methanol fuel cell application*, Polymers 10 (2018), https://doi.org/10.3390/polym10020194.
[54] N. Boulif, et al., Structure and performance of clay composite membranes with improved sodium conductivity for salinity gradient batteries, Appl. Clay Sci. 245 (2023) 107136, https://doi.org/10.1016/j.clay.2023.107136.
[55] L.B. de Paiva, A.R. Morales, F.R. Valenzuela Díaz, Organoclays: properties, preparation and applications, Appl. Clay Sci. 42 (1) (2008) 8–24, https://doi.org/10.1016/j.clay.2008.02.006.
[56] D. Amaya-Vías, E. Nebot, J.A. López-Ramírez, Comparative studies of different membrane distillation configurations and membranes for potential use on board cruise vessels, Desalination 429 (2018) 44–51, https://doi.org/10.1016/j.desal.2017.12.008.
[57] A. Hagedorn, et al., Membrane and spacer evaluation with respect to future module design in membrane distillation, Desalination 413 (2017) 154–167, https://doi.org/10.1016/j.desal.2017.03.016.
[58] A. Ali, et al., Progress in module design for membrane distillation, Desalination 581 (2024) 117584, https://doi.org/10.1016/j.desal.2024.117584.
[59] M. Huang, et al., Novel electrospun ZIF/PcH nanofibrous membranes for enhanced performance of membrane distillation for salty and dyeing wastewater treatment, Desalination 527 (2022) 115563, https://doi.org/10.1016/j.desal.2022.115563.
[60] B. Eryildiz, et al., Flux-enhanced reduced graphene oxide (rGO)/PVDF nanofibrous membrane distillation membranes for the removal of boron from geothermal water, Sep. Purif. Technol. 274 (2021) 119058, https://doi.org/10.1016/j.seppur.2021.119058.
[61] G. Vaghela, et al., Reinforced PS-PVDF-WO3 superhydrophobic antiwetting membrane for membrane distillation, Desalination 575 (2024) 117265, https://doi.org/10.1016/j.desal.2023.117265.
[62] M.O. Aijaz, et al., Electrospun bio-polymeric nanofibrous membrane for membrane distillation desalination application, Desalination 586 (2024) 117825, https://doi.org/10.1016/j.desal.2024.117825.
[63] W. Jankowski, W. Kujawski, J. Kujawa, Enhanced performance of electrospun PVDF membranes modified with rare-earth metal oxides for membrane distillation: A systematic study, Desalination 584 (2024) 117742, https://doi.org/10.1016/j.desal.2024.117742.
[64] M. Asadolahi, H. Fashandi, Endowing poly (vinylidene fluoride) membrane surface with Photothermal and Omniphobic properties through a single-step, electrospinning-based technique to enhance vacuum membrane distillation, Desalination 572 (2024) 117125, https://doi.org/10.1016/j.desal.2023.117125.
[65] A.S. Alsaadi, et al., Modeling of air-gap membrane distillation process: A theoretical and experimental study, J. Membr. Sci. 445 (2013) 53–65, https://doi.org/10.1016/j.memsci.2013.05.049.
[66] M.M. Damtie, et al., Membrane distillation for industrial wastewater treatment: studying the effects of membrane parameters on the wetting performance, Chemosphere 206 (2018) 793–801, https://doi.org/10.1016/j.chemosphere.2018.05.070.
[67] M.M. Damtie, J.-S. Choi, Modeling and application of direct contact membrane distillation for fluoride removal from aqueous solutions, Desalin. Water Treat. 97 (2017) 23–40, https://doi.org/10.5004/dwt.2017.21690.
[68] N.T.U. Kumar, A. Martin, Experimental modeling of an air-gap membrane distillation module and simulation of a solar thermal integrated system for water purification, Desalin. Water Treat. 84 (2017) 123–134, https://doi.org/10.5004/dwt.2017.21201.
[69] M. Qtaishat, et al., Heat and mass transfer analysis in direct contact membrane distillation, Desalination 219 (1) (2008) 272–292, https://doi.org/10.1016/j.desal.2007.05.019.
[70] J. Choi, et al., Exergy analysis of a direct contact membrane distillation (DCMD) system based on computational fluid dynamics (CFD), Membranes 11 (2021), https://doi.org/10.3390/membranes11070525.
[71] N.A.M. Ameen, et al., Highly saline water desalination using direct contact membrane distillation (DCMD): experimental and simulation study, Water 12 (2020), https://doi.org/10.3390/w12061575.